Acta Crystallographica Section D
Biological Crystallography
ISSN 0907-4449

Structure of an RNA dimer of a regulatory element from human thymidylate synthase mRNA

Sergey Dibrov,‡ Jaime McLean‡ and Thomas Hermann*

Department of Chemistry and Biochemistry, University of California, San Diego, 9500 Gilman Drive, La Jolla, CA 92093, USA

‡ These authors contributed equally.

Correspondence e-mail: tch@ucsd.edu

Received 30 October 2010
Accepted 4 December 2010

PDB Reference: TS1 dimer, 3mei.

NDB Reference: TS1 dimer, NA0505.

A sequence around the start codon of the mRNA of human thymidylate synthase (TS) folds into a secondary-structure motif in which the initiation site is sequestered in a metastable hairpin. Binding of the protein to its own mRNA at the hairpin prevents the production of TS through a translation-repression feedback mechanism. Stabilization of the mRNA hairpin by other ligands has been proposed as a strategy to reduce TS levels in anticancer therapy. Rapidly proliferating cells require high TS activity to maintain the production of thymidine as a building block for DNA synthesis. The crystal structure of a model oligonucleotide (TS1) that represents the TS-binding site of the mRNA has been determined. While fluorescence studies showed that the TS1 RNA preferentially adopts a hairpin structure in solution, even at high RNA concentrations, an asymmetric dimer of two hybridized TS1 strands was obtained in the crystal. The TS1 dimer contains an unusual S-turn motif that also occurs in the 'off' state of the human ribosomal decoding site RNA.

1. Introduction

Thymidylate synthase (TS) catalyzes the reductive methylation of 2′-deoxyuridine-5′-monophosphate (dUMP) to form 2′-deoxythymidine-5′-monophosphate (dTMP). Further phosphorylation of dTMP furnishes the triphosphate dTTP, which is essential for DNA synthesis and cellular proliferation. As the sole *de novo* pathway for dTTP synthesis, TS is an attractive cancer chemotherapy target (Chu *et al.*, 2003). 5-Fluorouracil (5-FU), one of the earliest anticancer agents to be used as a TS inhibitor, remains a mainstay in colorectal cancer therapy (Marsh, 2005). 5-FU serves as a prodrug that is metabolized to the active TS inhibitor 5-fluoro-2′-deoxyuridine-5′-monophosphate (FdUMP). As well as being incorporated into cellular DNA and RNA, FdUMP directly inhibits TS by forming a covalent ternary complex with the methyl-donor cofactor N^5,N^{10}-methylene tetrahydrofolate (mTHF; Chu *et al.*, 2003).

The efficient clinical use of 5-FU has been hampered by the rapid development of resistance to the drug through overexpression of TS (Chu *et al.*, 2003). In its unliganded and reduced form TS binds at two independent sites within its own mRNA and thereby downregulates its own translation (Fig. 1*a*; Chu *et al.*, 1993; Lin *et al.*, 2000). The formation of a ternary complex with either dUMP or FdUMP abolishes the mRNA-binding function of TS (Tai *et al.*, 2004). While similar feedback mechanisms are common in prokaryotic translation

regulation, TS expression is the first known example of translational autoregulation in mammalian cells (Chu *et al.*, 1991). TS protein binding at both mRNA sites is required for full translational repression (Lin *et al.*, 2000). Site 1 is predicted to fold into a hairpin loop that includes part of the 5′-untranslated region and continues into the coding region (Chu *et al.*, 1993). Upon protein binding to site 1, the start codon is sequestered within the hairpin and is unavailable for translation initiation. Stabilization of the site 1 mRNA hairpin by a small-molecule ligand, independent of TS binding, could inhibit protein production sufficiently to overcome 5-FU-dependent overexpression of the enzyme, ultimately enhancing the chemotherapeutic effect of 5-FU.

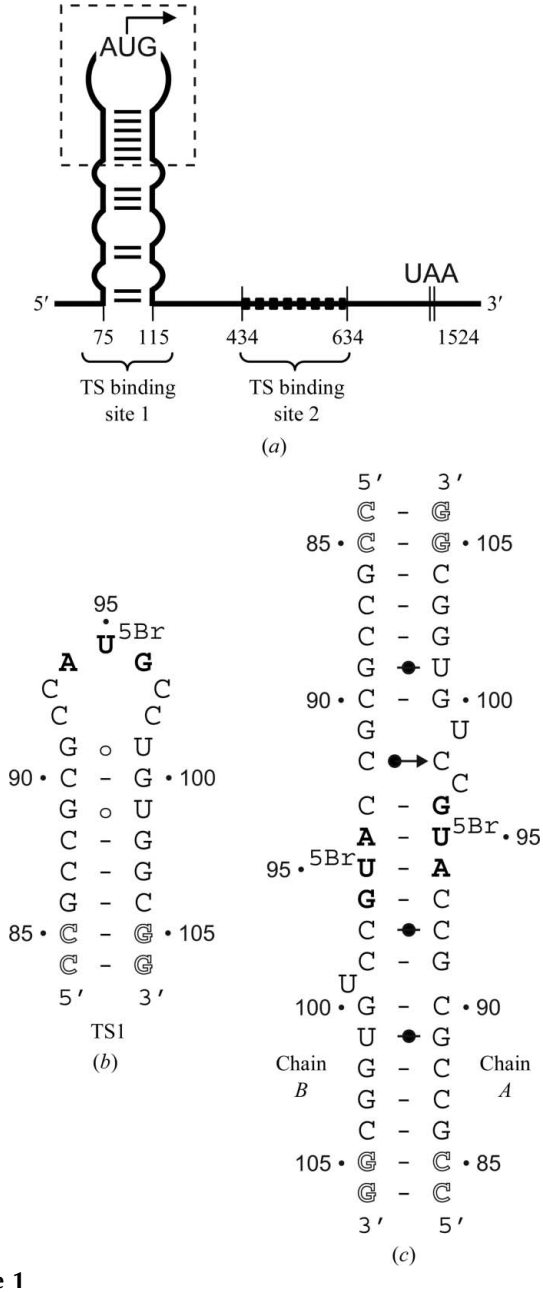

Figure 1
(*a*) Secondary structure of the human TS mRNA which contains two binding sites for the enzyme. Site 1 is predicted to adopt a hairpin structure around the AUG initiation codon (bold). Site 2 is located within the reading frame. Numbering is according to the *Homo sapiens* sequence (record NM_001071 of the NCBI Nucleotide Database; Takeishi *et al.*, 1985). (*b*) The 5-bromouridine (^{5Br}U)-labeled TS1 model construct used for crystallization. Residues that differ from the wild-type sequence are shown in outline. (*c*) Secondary structure of the TS1 RNA dimer as observed in the crystal. Symbols indicating non-Watson–Crick base-pair interactions are according to the Leontis–Westhof annotation (Leontis & Westhof, 2001).

To support our efforts in ligand discovery for the site 1 target, we are investigating synthetic oligonucleotide models of the mRNA hairpin. Crystals diffracting to 1.97 Å resolution were obtained for the 5-bromouridine-labeled 23 nt TS1 RNA (Fig. 1*b*), an oligonucleotide that has been shown to bind the TS protein. Structure determination by X-ray crystallography revealed that the TS1 RNA had crystallized as an asymmetrical dimer of two oligonucleotide strands rather than in the desired hairpin configuration (Fig. 1*c*). In contrast, fluorescence labeling studies demonstrated that in solution the TS1 RNA preferentially adopts a stable hairpin fold. The transition of RNA hairpin structures to homodimers at high RNA and salt concentrations, which are typical of crystallization conditions, has been observed previously (Holbrook *et al.*, 1991; Bevilacqua & Blose, 2008). Unlike other hairpin RNAs that crystallized as dimers, the TS1 oligonucleotide adopts a unique asymmetrical dimer structure that contains multiple non-Watson–Crick base pairs and bulged-out residues (Fig. 1*c*).

2. Materials and methods

2.1. RNA constructs

Synthetic desalted TS1 oligonucleotide (5′-CCG CCG CGC CAU[5Br] GCC UGU GGC GG-3′) for crystallization was obtained from Dharmacon (Lafayette, Colorado, USA). HPLC-purified oligonucleotides for fluorescence studies (TS1, TS1-Fl, TS-FlQ, TS1-Q, TS1-C and TS1-CQ; see Figs. 2 and 3 and §2.2) were purchased from IDT (Coralville, Iowa, USA).

2.2. Solution fluorescence studies

Fluorescence measurements were performed on a thermostatted RF-5301PC spectrofluorometer (Shimadzu, Columbia, Maryland, USA) at 298 K. Emission spectra of TS1-Fl (5′-CCG CCG CGC CAU GCC UGU GGC GG-3′-fluorescein) were recorded in 10 m*M* sodium cacodylate buffer pH 6.5 at 135 n*M* RNA concentration (excitation 492 nm, emission 520 nm). Either 135 n*M* (1×) or 1.35 µ*M* (10×) unlabeled TS1 RNA, TS1-Q (DABCYL-5′-CCG CCG CGC CAU GCC UGU GGC GG-3′), TS1-C (5′-CCG CCA CAG GCA UGG CGC GGC GG-3′) or TS1-CQ (DABCYL-5′-CCG CCA CAG GCA UGG CGC GGC GG-3′) was added [DABCYL = 4-(dimethylaminoazo)benzene-4-carboxylic acid]. The RNA was incubated at 348 K for 5 min in the absence of salt or in the presence of 100 m*M* NaCl or 10 m*M* $MgCl_2$. The RNA was then cooled on ice for 5 min and fluorescence readings were recorded continually for 10 min. For fluorescence experiments at RNA concentrations that were comparable to the crystallization conditions (Fig. 3), the fluorescence of TS1-FlQ (DABCYL-5′-CCG CCG CGC CAU GCC UGU GGC GG-

3′-flourescein) was measured at 0.4 µ*M* RNA concentration in the different salt conditions mentioned above, annealed in the absence and presence of either 1.2 µ*M* TS1-C, 150 µ*M* unlabeled TS1 or 150 µ*M* tRNA (total tRNA from *Saccharomyces cerevisiae*; Sigma, St Louis, Missouri, USA).

2.3. RNA crystallization

Lyophilized 5-bromouridine-labeled TS1 RNA was dissolved in 10 m*M* sodium cacodylate buffer pH 6.5 at a concentration of 300 µ*M*. The RNA was annealed by heating to 338 K for 3 min followed by immediate cooling on ice. Crystals grew within 2–5 d at room temperature in hanging drops consisting of 1 µl 300 µ*M* RNA and 1 µl precipitant solution (50 m*M* sodium cacodylate pH 6.5, 30–50 m*M* $MgCl_2$, 10–12% 2-methyl-2,4-pentanediol) which were equilibrated by vapor diffusion against a reservoir containing 500 µl of identical precipitant solution.

2.4. Diffraction data collection and structure determination

Crystals were cryoprotected by soaking them for 5 s in the original reservoir solution containing 15%(*v*/*v*) PEG 200, flash-cooled in liquid nitrogen and transferred to a cold nitrogen stream. The structure of TS1 RNA was determined by single-wavelength anomalous dispersion (SAD) phasing using the anomalous scattering from a Br atom incorporated at U95. Two Br atoms were present per TS1 oligonucleotide dimer. A SAD data set was collected at 100 K on beamline 17-ID-B at the Advanced Photon Source (APS), Argonne National Laboratory (Illinois, USA). 250 images were recorded at a crystal-to-detector distance of 180 mm using an exposure time of 10 s per frame with 1° oscillation. Data were processed, integrated and scaled with the *HKL*-2000 package (Otwinowski & Minor, 1997). Initial phases were calculated from the SAD data of the brominated RNA derivative using the *CNS* suite of programs (Brünger *et al.*, 1998; Brunger, 2007). A Patterson search revealed the positions of two independent Br atoms, based on which an initial electron-density map was calculated. The map was of sufficient quality to allow the building of an initial three-dimensional structure model using the *Coot* software (Emsley & Cowtan, 2004). Iterative rounds of model building and refinement were performed, alternating between the *REFMAC* program (Murshudov *et al.*, 1997) within the *CCP*4 package (Collaborative Computational Project, Number 4, 1994) and *Coot*, until a complete RNA dimer was built. The complete structure was further refined by rigid-body refinement and multiple rounds of restrained minimization in *REFMAC* as well as manual rebuilding in *Coot* guided by the $2F_o - F_c$ and $F_o - F_c$ electron-density maps. During this refinement step five magnesium ions were placed into the electron-density maps. The progress of model rebuilding and refinement was monitored by the R_{free} parameter, which was calculated from a randomly chosen test set comprising 4.6% of the data. A final refinement round was carried out with the *PHENIX* software (Adams *et al.*, 2002) using combined TLS and individual isotropic atomic displacement parameters with a phased maximum-likelihood target. During the last cycles, the water-picking protocol in *PHENIX* was added. The refined structure has been deposited into the Protein Data Bank (code 3mei) and the Nucleic Acid Database (code NA0505). Data-collection and refinement statistics are given in Table 1.

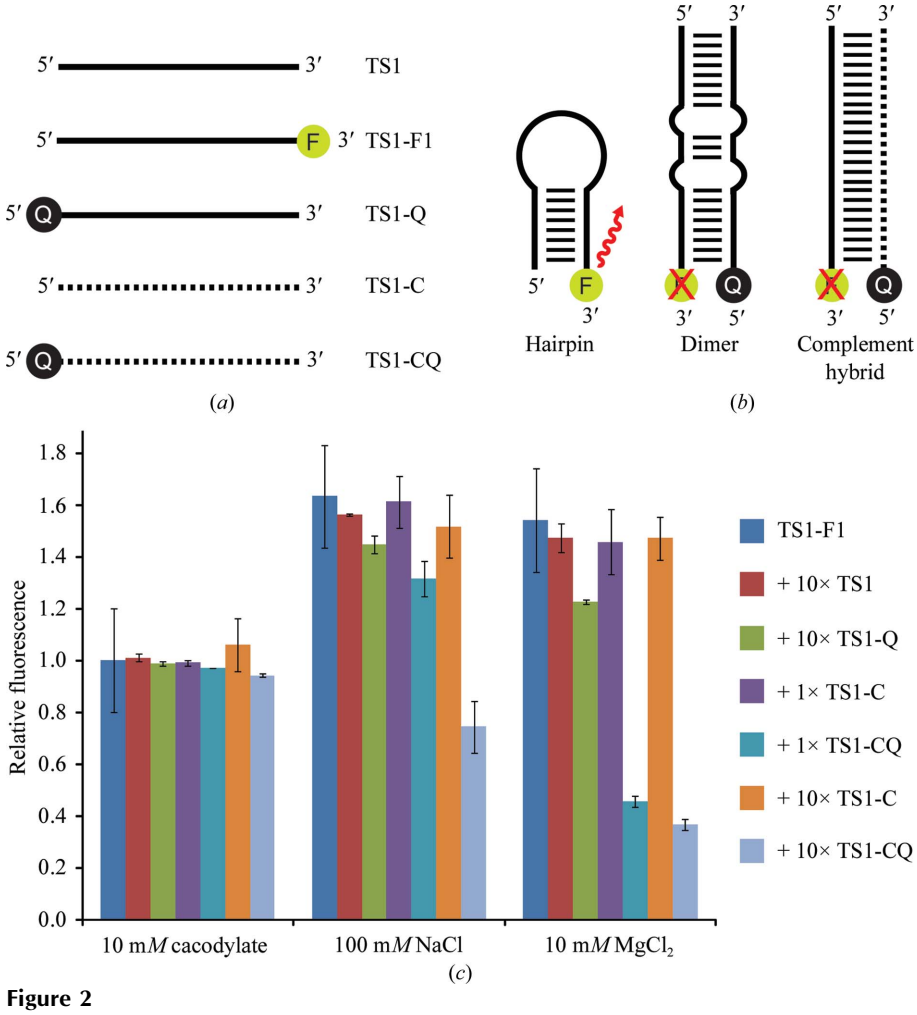

Figure 2
(*a*) Oligonucleotides used for solution fluorescence studies on the TS1 RNA. TS1, unmodified RNA; TS1-Fl, 3′ fluorescein labeled; TS1-Q, 5′-labeled with DABCYL quencher; TS1-C, exact complement to TS1 RNA; TS1-CQ, complement 5′-labeled with DABCYL quencher. (*b*) Selected RNA species that may form in mixtures of the TS1 oligonucleotides. Fluorescence is reduced when the fluorescein label and DABCYL quencher are adjacent in the dimer and complement hybrid. (*c*) Fluorescence observed in annealed mixtures of the TS1 oligonucleotides. See text for discussion.

3. Results and discussion

3.1. Solution fluorescence studies of TS1 RNA

To determine whether the TS1 RNA adopted a hairpin or dimer configuration in solution, we investigated fluorescently labeled TS1 oligonucleotides which were annealed in the presence of salt (Fig. 2). In the absence of salt the TS1 RNA did not adopt a stably folded structure and the fluorescence of a 3′ fluorescein-labeled TS1 oligonucleotide (TS-Fl) was unaffected by the presence of other RNA. When TS1-Fl was annealed in the presence of a tenfold excess of a 5′ DABCYL quencher-linked RNA (TS1-Q) only a small reduction in fluorescence was observed, suggesting that a major fraction of both oligonucleotides folded individually into the hairpin structure. In the hairpin fold the fluorescein label is freely exposed to solvent and gives rise to a high fluorescence signal (Fig. 2). Fluorescence was strongly reduced when TS1-Fl was annealed with either a stoichiometric amount or a tenfold excess of a fully complementary oligonucleotide that carried a 5′ DABCYL quencher (TS1-CQ). In the mixture with the complementary strand the double-stranded hybrid is the thermodynamically most stable species in which the fluorescein label and DABCYL quencher are adjacent, leading to fluorescence quenching (Fig. 2). The same effect would occur in a mixture of TS1-Fl and TS1-Q if the TS1 dimer was the preferred configuration in solution. Since fluorescence was only minimally affected in this case, we conclude that the TS1 RNA preferentially adopted a hairpin fold in solution. A decrease in fluorescence was not observed in control experiments in which TS1-Fl was annealed with an excess of unlabeled TS1 and fully complementary TS1-C.

While the fluorescence experiments only required nanomolar samples of fluorescein-labeled TS1 RNA, crystallization conditions are typically conducted at higher RNA concentrations in the micromolar range. To rule out an effect of the high RNA concentrations used in crystallization trials on the potential equilibrium between the hairpin and dimer configurations of the TS1 RNA, we performed fluorescence trace labeling experiments (Fig. 3). A doubly labeled TS1 oligonucleotide (TS1-FlQ) which carried a 5′ fluorescein dye as well as a 3′ DABCYL quencher gave only low fluorescence at 400 n*M* concentration, indicating that the RNA adopted a hairpin structure in which the terminal dye and quencher were in proximity. The fluorescence increased over 30-fold when fully complementary TS1-C was added, which allowed the formation of the complement hybrid in which the labeled termini of TS1-FlQ were at a maximum distance and quenching of the fluorescein signal was released. The addition of a large excess of unlabeled TS1 RNA (150 µ*M*) before annealing did not lead to a significant increase in fluorescence (Fig. 3), suggesting that the hairpin configuration is preferred in solution even at the RNA concentrations used in crystallization trials. Similarly, the addition of an unrelated RNA (total tRNA) at high concentration did not affect the fluorescein quenching in the TS1-FlQ oligonucleotide.

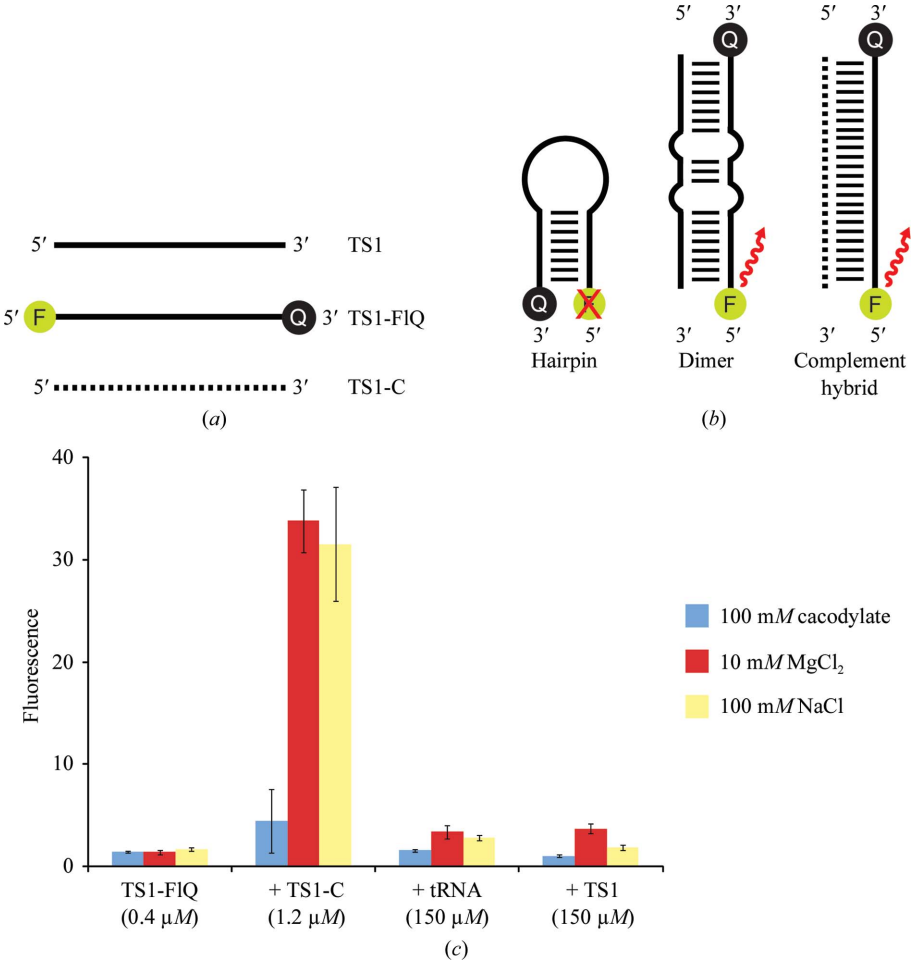

Figure 3
(*a*) Oligonucleotides used for solution fluorescence studies on the TS1 RNA at high RNA concentrations that correspond to the crystallization conditions. TS1, unmodified RNA; TS1-FlQ, 5′-labeled with fluorescein and 3′-labeled with DABCYL quencher; TS1-C, exact complement to TS1 RNA. (*b*) Selected RNA species that may form in mixtures of the TS1 oligonucleotides. Fluorescence is abolished in the hairpin structure, when the fluorescein label and DABCYL quencher are adjacent, and is enhanced in the dimer and complement hybrid, when the dye and quencher are spatially separated. (*c*) Fluorescence observed in annealed mixtures of TS1 oligonucleotides. See text for discussion.

3.2. Crystal structure of the TS1 RNA dimer

While the TS1 RNA preferentially folds into a hairpin in solution, dimerization of the oligonucleotide was observed in the crystal. The three-dimensional structure of the TS1 RNA

determined at 1.97 Å resolution by single-wavelength anomalous diffraction revealed an asymmetric dimer of two base-paired TS1 strands adopting an overall double-helical architecture (Fig. 4). In the crystal, the TS1 RNA dimer helices are aligned in a pseudo-continuous end-to-end arrangement that is stabilized by stacking of the closing base pairs. The two TS1 oligonucleotides in the dimer form an asymmetrical helix with a prominent S-turn motif in the sugar phosphate backbone of one strand (*A*) located at $C97_A$–$U99_A$ that is absent in the other strand (*B*) (Fig. 4). Capture in the crystal of two conformational states of identical sequences within a dimer has commonly been observed for oligonucleotide models of the ribosomal decoding site (Kondo, Urzhumtsev *et al.*, 2006; Kondo & Westhof, 2008). In the TS1 dimer, the first seven base pairs at both ends form canonical A-form helices of standard Watson–Crick and G·U wobble base pairs ($C84_{A/B}$–$G106_{B/A}$ through $C90_{A/B}$–$G100_{B/A}$). A-form Watson–Crick pairs are also found at the center of the dimer, $C93_A$–$G96_B$ through $G96_A$–$C93_B$, which includes the 5-bromouridines at positions $95_{A/B}$.

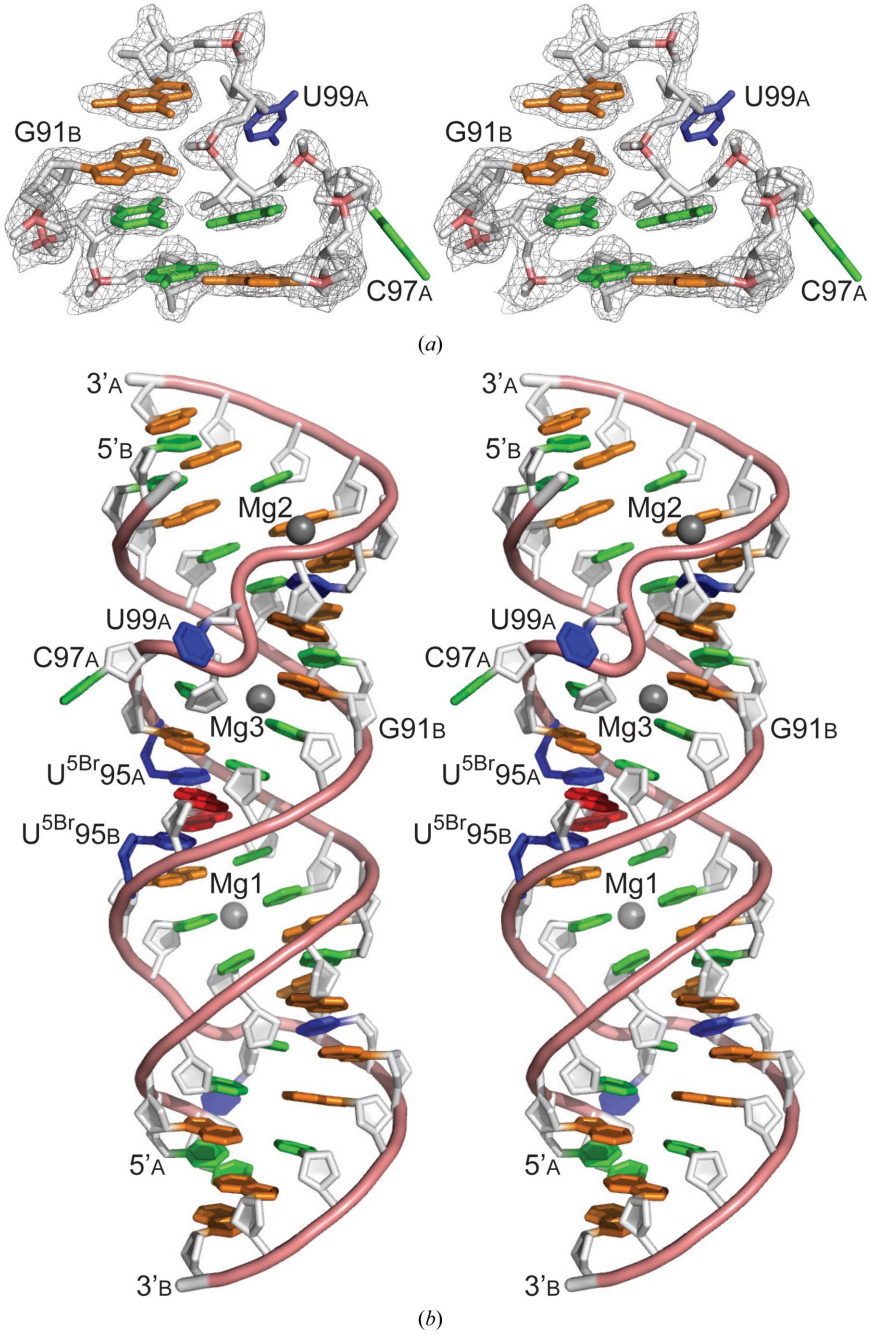

Figure 4
(*a*) Stereoview of an OMIT $F_o - F_c$ electron-density map, contoured at 2σ, around the S-turn of the TS1 RNA dimer. Shown are residues G96–G100 in chain *A* and G91–C93 in chain *B* (see also Fig. 6), which were removed from the model for calculation of the map. (*b*) Overall structure of the TS1 RNA dimer. Bases are colored according to the sequence: A, red; C, green; G, orange; U, blue. Magnesium ions are shown as gray spheres.

At one end of the TS1 dimer (bottom in Fig. 1*c*), the base $U99_B$ is rotated out from the RNA duplex and participates in intermolecular crystal-packing contacts (Fig. 5). The O4 carbonyl atom of the $U99_B$ base forms a hydrogen bond with the 3′-hydroxyl group of the $G106_A$ ribose in the terminal base pair of a neighboring RNA helix. This interaction, together with a second intermolecular hydrogen bond between HN3 of $U99_B$ and O1P of the same $G106_A$, leads to decreased thermal parameters for $U99_B$ compared with other extrahelical bases. The average *B* factor of the $U99_B$ base is 49 Å^2. Flanking the $U99_B$ residue are base pairs $G91_A$–$C98_B$ and $C90_A$–$G100_B$, which are twisted relative to each other such that $G91_A$ stacks over the center of the $C90_A$–$G100_B$ pair, while $C98_B$ is shifted into the major groove. Above $G91_A$–$C98_B$, a non-canonical base pair is formed between $C92_A$·$C97_B$, which adopt a *cis*-Watson–Crick/Watson–Crick geometry (Leontis & Westhof, 2001).

On the other side of the RNA duplex (top in Fig. 1*c*), the stretch of bases $C97_A$ to $U99_A$ adopts a distinct S-turn motif (Figs. 4 and 6), which is different from the *B* strand and leads to the overall asymmetrical architecture of the TS1 dimer. Like $U99_B$, $U99_A$ is rotated out from the duplex but unlike its counterpart in the *B* strand this uridine does not form crystal-packing contacts with a neighboring helix. As a consequence, the base of $U99_A$ is disordered and displays high thermal parameters (average *B* factor of 73 Å^2). The phosphate group of $U99_A$ is twisted such that the phosphate O atoms point inside the RNA duplex, where they engage in two hydrogen bonds to $G91_B$: O2P with HN1 and O1P with HN2. At the center of the S-turn $C98_A$ docks with its sugar edge at the Watson–Crick face of $C92_B$ to form a *cis*-Watson–Crick/sugar edge base pair (Leontis & Westhof, 2001). The third residue of the S-turn, $C97_A$, is stabilized in a

Table 1
Data-collection and refinement statistics for TS1 RNA.

Values in parentheses are for the highest resolution shell.

Data collection	
Wavelength (Å)	0.91970
High-resolution limit (Å)	1.97
Low-resolution limit (Å)	28.2
Multiplicity	8.5 (2.7)
Completeness (%)	97.8 (81.9)
$\langle I/\sigma(I)\rangle$	25.28 (5.87)
$R_{\rm meas}$ (%)	7.1 (28.5)
Total reflections	62295
Unique reflections	7328
Refinement	
Space group	$P2_1$
Unit-cell parameters	
a (Å)	32.93
b (Å)	38.56
c (Å)	41.99
β (°)	100.10
$R_{\rm work}/R_{\rm free}$	0.176/0.238
No. of atoms	
RNA atoms	974
Solvent atoms	132
Metal ions	3 Mg^{2+}
Mean B factors (Å^2)	
RNA	31.8
Solvent	42.9
Metal	62.3
R.m.s. deviations	
Bond lengths (Å)	0.015
Bond angles (°)	2.28
Dihedral angles (°)	16.72

conformation rotated out of the RNA duplex by a hydrogen-bond interaction of its O2P phosphate oxygen with the N4 amino group of $C98_A$. The base of $C97_A$ points into the major groove of a neighboring RNA helix in a region between the phosphate groups of $C104_B$ and $G105_B$, which restrict the thermal motion of $C97_A$ (average B factor of 58 Å^2).

3.3. Magnesium binding sites in the TS1 RNA dimer

Guided by electron density and coordination geometry as well as optimization of $R/R_{\rm free}$, three Mg^{2+} cations were placed in the crystal structure of the TS1 dimer (Fig. 4*b*). Mg1 is bound in the minor groove and coordinates five water molecules in a square-pyramidal orientation with distances to O atoms of 2.1–2.3 Å. Mg2 and Mg3 are located inside the major groove of the RNA helix. Mg2 is positioned between the planes of the $G102_A$–$C88_B$ and $G103_A$–$C87_B$ base pairs at 3.2 and 4.0 Å away from the N7 atoms of $G102_A$ and $G103_B$, respectively. The O2P O atom of $G102_A$ is at a distance of 3.9 Å from Mg2. Two water molecules complete its coordination sphere at distances of 2.0 and 2.2 Å. Mg3 is equidistant from the Hoogsteen edge N7 atom of $G91_B$ and the N3 atom of $C98_A$, with the N—Mg distance being 4.6 Å in both cases. Mg3 makes close contacts with three water molecules, with an average O—Mg distance of 2.3 Å. None of the magnesium ions participate in intermolecular crystal-packing contacts.

3.4. Comparison of the TS1 dimer with other RNA structures

The TS1 dimer contains an S-turn motif which is comprised of residues $C97_A$ to $U99_A$ in the *A* strand and $G91_B$ to $C92_B$ in the *B* strand. The S-turn is flanked by the regular Watson–Crick base pairs $G96_A$–$C93_B$ and $G100_A$–$C90_B$. Surprisingly, the geometry of this region, including the flanking pairs, in the TS1 RNA resembles the structure of the human cytoplasmic ribosomal decoding site in the 'off' state (Kondo, Urzhumtsev *et al.*, 2006; Kondo, Francois *et al.*, 2006), despite there being no sequence similarity between the RNAs (Fig. 7). The central $C98_A$·$C92_B$ pair of the TS1 dimer superimposes on the C1409·A1492 pair in the human decoding site, both of which align with a *cis*-Watson-Crick/sugar edge geometry. The two rotated-out pyrimidine bases $C97_A$ and $U99_A$ in the TS1 dimer

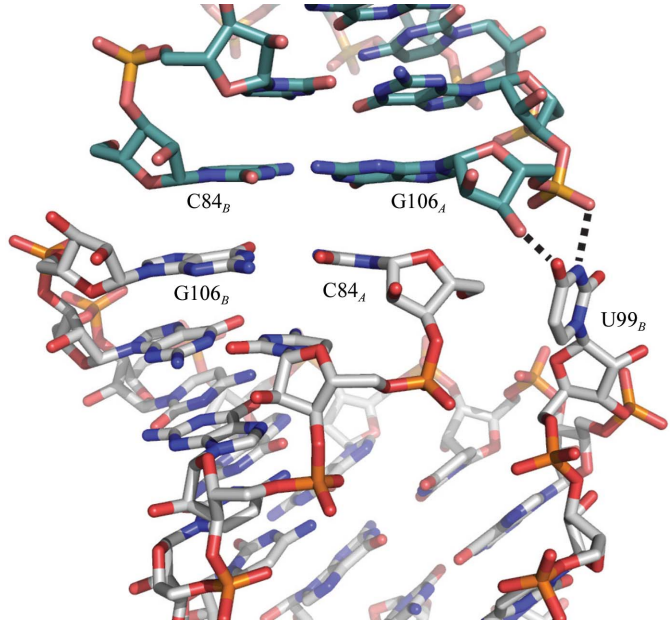

Figure 5
Pseudo-continuous end-to-end arrangement of TS1 RNA dimer helices in the crystal. Hydrogen bonds between two neighboring helices are indicated as dashed lines.

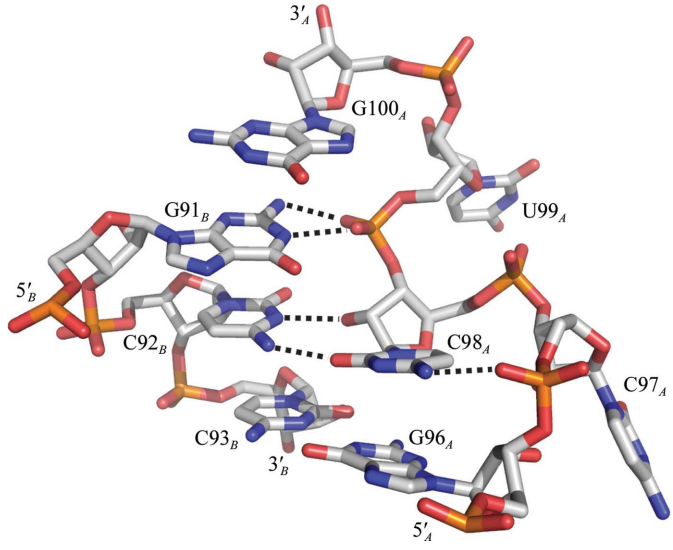

Figure 6
Geometry of the S-turn in the stretch of bases $C97_A$ to $U99_A$ in strand *A* of the TS1 RNA dimer. Hydrogen bonds are indicated as dashed lines.

adopt similar conformations as the extrahelical adenines A1491 and A1493 in the ribosomal RNA. The Watson–Crick pairs $G96_A$–$C93_B$ and $G100_A$–$C90_B$ flanking the TS1 S-turn correspond to the A1490–U1410 and G1494–C1407 pairs in the human decoding site. The r.m.s.d. of the superimposed TS1 dimer and human decoding site RNA in the region of the S-turn, including the flanking pairs, is 0.97 Å.

The surprising similarity of the S-turns in the decoding site and the TS1 dimer again demonstrates how the modular architecture of RNA folds allows the formation of identical structural motifs in unrelated sequence contexts. This finding further emphasizes the importance of tertiary-structure modules for the assembly as well as the description of complex RNA folds (Hermann & Patel, 1999).

4. Summary and future studies

The structure of the TS1 model oligonucleotide, which represents a regulatory motif in the mRNA of the human TS enzyme, revealed the formation of an asymmetric homodimer rather than the expected hairpin motif. While crystallization as a dimer has been frequently observed for other hairpin RNA sequences, fluorescence labeling studies on the TS1 oligonucleotide at concentrations that resemble the crystallization conditions suggest that this RNA does indeed form a hairpin in solution. In future studies, several routes will be explored to prevent dimer formation in the crystal. We are currently crystallizing modified TS1 constructs that have extended stable stem sequences which are aimed at reducing the impact of the hairpin on crystallization. Furthermore, we are studying fusion constructs of the TS1 hairpin joined to an RNA sequence that serves as a binding site for the spliceosomal protein U1A, which has been successfully used to crystallize native folds of RNA (Ferré-D'Amaré & Doudna, 2000; Ferré-D'Amaré, 2010).

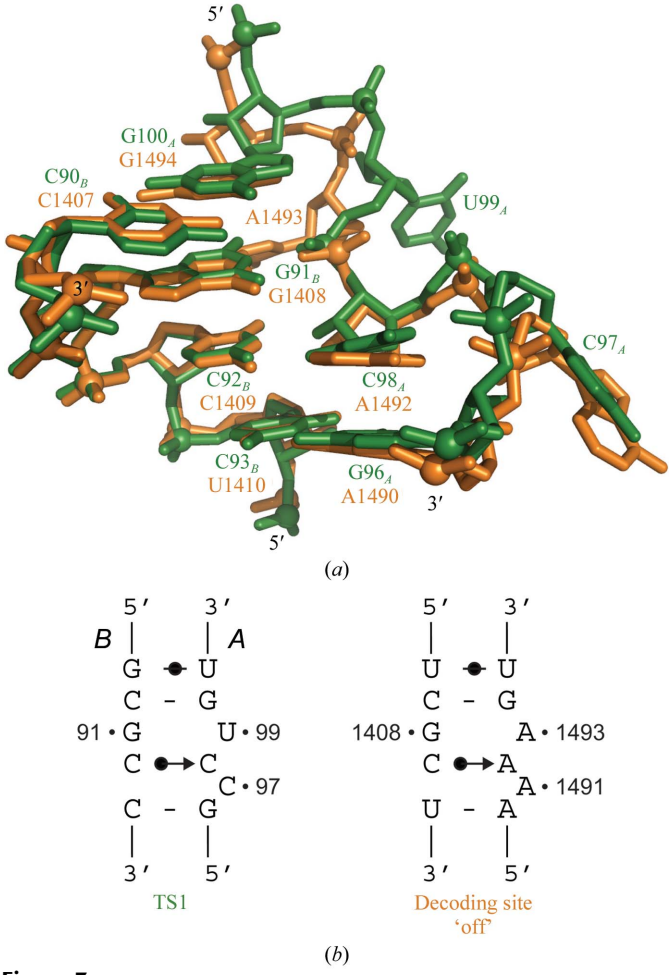

Figure 7
(*a*) Superposition of the S-turn motif in the TS1 RNA dimer (green) and the human cytoplasmic ribosomal decoding site in the 'off' state (orange) (Kondo, Urzhumtsev *et al.*, 2006; Kondo, Francois *et al.*, 2006). (*b*) Secondary-structure and sequence comparison of the TS1 and decoding site S-turn motifs.

We thank Dr Ganapathy Sarma for help with data processing. This work was supported in part by the National Institutes of Health (grant No. CA132753). Use of the Advanced Photon Source was supported by the US Department of Energy, Office of Science, Office of Basic Energy Sciences under Contract No. DE-AC02-06CH11357. Use of the IMCA-CAT beamline 17-ID at the Advanced Photon was supported by the companies of the Industrial Macromolecular Crystallography Association through a contract with the Center for Advanced Radiation Sources at the University of Chicago.

References

Adams, P. D., Grosse-Kunstleve, R. W., Hung, L.-W., Ioerger, T. R., McCoy, A. J., Moriarty, N. W., Read, R. J., Sacchettini, J. C., Sauter, N. K. & Terwilliger, T. C. (2002). *Acta Cryst.* D**58**, 1948–1954.
Bevilacqua, P. C. & Blose, J. M. (2008). *Annu. Rev. Phys. Chem.* **59**, 79–103.
Brunger, A. T. (2007). *Nature Protoc.* **2**, 2728–2733.
Brünger, A. T., Adams, P. D., Clore, G. M., DeLano, W. L., Gros, P., Grosse-Kunstleve, R. W., Jiang, J.-S., Kuszewski, J., Nilges, M., Pannu, N. S., Read, R. J., Rice, L. M., Simonson, T. & Warren, G. L. (1998). *Acta Cryst.* D**54**, 905–921.
Chu, E., Callender, M. A., Farrell, M. P. & Schmitz, J. C. (2003). *Cancer Chemother. Pharmacol.* **52**, S80–S89.
Chu, E., Koeller, D. M., Casey, J. L., Drake, J. C., Chabner, B. A., Elwood, P. C., Zinn, S. & Allegra, C. J. (1991). *Proc. Natl Acad. Sci. USA*, **88**, 8977–8981.
Chu, E., Voeller, D., Koeller, D. M., Drake, J. C., Takimoto, C. H., Maley, G. F., Maley, F. & Allegra, C. J. (1993). *Proc. Natl Acad. Sci. USA*, **90**, 517–521.
Collaborative Computational Project, Number 4 (1994). *Acta Cryst.* D**50**, 760–763.
Emsley, P. & Cowtan, K. (2004). *Acta Cryst.* D**60**, 2126–2132.
Ferré-D'Amaré, A. R. (2010). *Methods*, **52**, 159–167.
Ferré-D'Amaré, A. R. & Doudna, J. A. (2000). *J. Mol. Biol.* **295**, 541–556.
Hermann, T. & Patel, D. J. (1999). *J. Mol. Biol.* **294**, 829–849.
Holbrook, S. R., Cheong, C., Tinoco, I. Jr & Kim, S.-H. (1991). *Nature (London)*, **353**, 579–581.
Kondo, J., Francois, B., Urzhumtsev, A. & Westhof, E. (2006). *Angew. Chem. Int. Ed. Engl.* **45**, 3310–3314.
Kondo, J., Urzhumtsev, A. & Westhof, E. (2006). *Nucleic Acids Res.* **34**, 676–685.
Kondo, J. & Westhof, E. (2008). *Nucleic Acids Res.* **36**, 2654–2666.
Leontis, N. B. & Westhof, E. (2001). *RNA*, **7**, 499–512.

Lin, X., Parsels, L. A., Voeller, D. M., Allegra, C. J., Maley, G. F., Maley, F. & Chu, E. (2000). *Nucleic Acids Res.* **28**, 1381–1389.
Marsh, S. (2005). *Invest. New Drugs*, **23**, 533–537.
Murshudov, G. N., Vagin, A. A. & Dodson, E. J. (1997). *Acta Cryst.* D**53**, 240–255.
Otwinowski, Z. & Minor, W. (1997). *Methods Enzymol.* **276**, 307–326.
Tai, N., Schmitz, J. C., Liu, J., Lin, X., Bailly, M., Chen, T. & Chu, E. (2004). *Front. Biosci.* **9**, 2521–2526.
Takeishi, K., Kaneda, S., Ayusawa, D., Shimizu, K., Gotoh, O. & Seno, T. (1985). *Nucleic Acids Res.* **13**, 2035–2043.